

Impact of Gap/Load Spacing on the Aerodynamic Performance of Intermodal Freight Trains

C. Li¹, M. Kost², D. Burton¹, J. Sheridan¹ and M. C. Thompson¹

¹Fluids Laboratory for Aeronautical and Industrial Research (FLAIR)
Department of Mechanical and Aerospace Engineering
Monash University, Victoria 3800, Australia

²Business Improvement Manager
Pacific National Rail, Victoria 3004, Australia

Abstract

The influence of load spacing variation on the aerodynamic drag of an intermodal freight train is investigated in the 450 kW Monash University wind tunnel. The model train consists of 7 wagons; each wagon modelled after generic 1/14.6th-scale double-stacked container wagons. The middle wagon is pressure tapped to record the pressure on the front and rear surfaces. The remaining wagons are un-instrumented and used to control upstream and downstream airflow so that it is similar to a long train. The aerodynamics is investigated as a function of the gaps upstream and downstream of the middle wagon. Experimental results indicate that the sectional drag is sensitive to gap size variations. The front and rear gap influences on the drag appear relatively independent of each other. Surface flow visualisation on the top of the load reveals two reattachment lines, the product of a series of recirculations located near the leading edge of the top surface.

Introduction

To improve the fuel efficiency of an intermodal freight train, reducing aerodynamic drag is important. A key feature of intermodal freight transport is the numerous loading combinations that are possible in the placement of freight containers on the train. This loading pattern will affect the overall drag. The direct effect of different loading patterns is the varying load spacing it introduces. A study by Lai et al. [5] illustrates the numerous ways that load spacing may be introduced. Drag growth is correlated with an increase of load spacing: a study by Engdahl et al. [1] on a full-scale train concludes that a significant drag increase occurs between a gap spacing of approximately 0.42 W to 0.73 W, where W is the width of the wagon. It is theorised that for larger gap spacings, train surface boundary layers have difficulty bridging the gap, thereby reinitiating on the downstream wagon. A study conducted by Watkins et al. [11] displays the drag growth experienced as the carriage spacing between gondola and hopper wagons are increased, and it is shown that the drag is further exacerbated by the introduction of crosswind.

Because of its extreme aspect ratio, it is difficult to model an entire train experimentally, and understanding the drag on any particular train does not necessarily help to predict the drag of another train with a different loading pattern. Therefore, a logical approach is to study the aerodynamics of an arbitrary wagon, assuming that the drag of an entire train can be obtained approximately through a linear summation of the drag contributions of individual wagons. In addition, it may be possible to develop an algorithm to minimise the drag of the entire train by determining the ideal loading pattern for a given collection of freight. Indeed, research of Lai et al. [6] has been directed towards achieving this goal by suggesting an algorithm to reduce the overall drag by decreasing the total number of gaps within the train, and by placing smaller gap sizes towards the front of

the train. However, further work in this area is certainly warranted. In this current study, the effect of gap spacing on the pressure distribution and surface flow structure of a representative container wagon will be investigated.

Experimental setup



Figure 1: Experimental setup in the 450 kW wind tunnel.

The experiments were conducted in the Monash University 450 kW wind tunnel, with a closed test section of 12 m × 2 m × 2 m. A false floor with a sharp wedge leading edge was placed 438 mm above the tunnel floor to remove the oncoming boundary layer. A 1/14.6th-scale model train consisting of 7 wagons was used, with each wagon modelled after a generic flatbed-trailer that was double-stacked with 48ft long containers. The tunnel speed of 30 m/s was maintained for all tests, which gave a Reynolds number of $Re = 3.27 \times 10^5$, based on train width. All wagons were aligned and facing the wind. Measurements were conducted on a test wagon located at the centre of the 7-wagon configuration (4th wagon from the front). The boundary layer thickness at the leading edge of the test wagon was 57% of the wagon height, and the tunnel blockage caused by the train was 2.4%. The 3 wagons in front and behind the test wagon were all non-instrumented dummy models.

According to past research, variation of aerodynamic drag with respect to the wagon's position reaches equilibrium if a wagon was a certain distance away from the nose and the tail of the train. Full-scale gondola testing conducted in 1987 [2] showed that the drag on a closed top gondola wagon reduced rapidly as the position in train was shifted downstream from the leading edge, eventually reaching a constant value at approximately the 8th position in the train. Wind tunnel experiments of Watkins et al. [11] indicated that no change in drag was observed in a test wagon once there were more than 1.5 wagons upstream and 0.5 wagons downstream. Numerical analysis conducted by Golo-

vanevskiy et al. [3] indicated that for 10, 12 and 14 wagon models, excluding the 3 wagons at the front and the rear, the series of wagons in the middle of the train displayed similar values of drag coefficient. Based on those knowledge, 7 wagons setup was employed for this project.

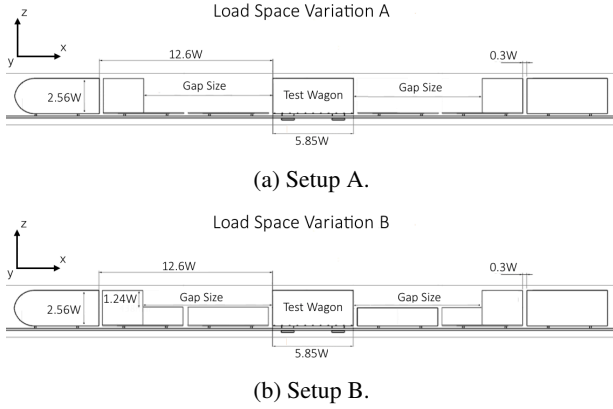


Figure 2: Side-view schematic of the two model setups.

A schematic of the model setup is displayed in figure 2, with all dimensions normalised by wagon width, $W = 171$ mm. The coordinate x is the longitudinal downstream direction with its origin at the nose of the train. Coordinate y points in the lateral direction towards the train's right, with its origin at the centre plane. Coordinate z points upwards in the vertical direction with its origin at the false floor. The primary variables are the front and rear load spacing size. Note that when the front gap size was varied, the rear gap size was maintained at a constant baseline value of $0.3 W$, and similarly, when the rear gap size was varied, the front gap was also maintained at a constant $0.3 W$. Spacing setup A and B shown in figure 2 are the gaps produced by removing of double-stacked or a single-stacked wagon respectively. As the intention is to study the aerodynamic impact of inter-load gap spacing, components adding complexity such as wheels, bogies and under-carriage features are not included in the models.

“Kaolin” china clay dyed with an orange fluorescent pigment was used for the purpose of surface flow visualisation. A mixture of clay with kerosene was applied onto the surface of the model. The kerosene acts as a medium for the clay particles to move freely on the surface. During experiments, a wind speed of 30 m/s was maintained for 2 minutes to allow the kerosene to fully evaporate. The flow image of the attached clay particles was then enhanced using a UV lamp. There was difficulty obtaining meaningful flow visualisation on the vertical surfaces of the model due to the influence of gravity.

A total of 106 pressure taps were positioned on the front and base surfaces of the test wagon. Since no crosswind was present during testing, the pressure distribution was expected to be symmetric about the middle plane. On each of the surfaces, 49 taps were located on one half of the surface to achieve higher tap density. Additionally, 4 taps were located on the other side of the symmetry line to check that symmetry was maintained. Two dynamic pressure measuring systems (DPMS) were mounted inside the model, with each DPMS capable of reading up to 64 channels. The dynamic pressure was determined from an upstream pitot static tube with a factor applied to correct its value to the test wagon's position ($x = 3156$ mm, $y = 0$ mm, $z = 500$ mm). The static pressure was referenced to the location of the upstream pitot static tube. Pressure data were recorded for a sampling time of 60 s at a sampling rate of 500 Hz. The pres-

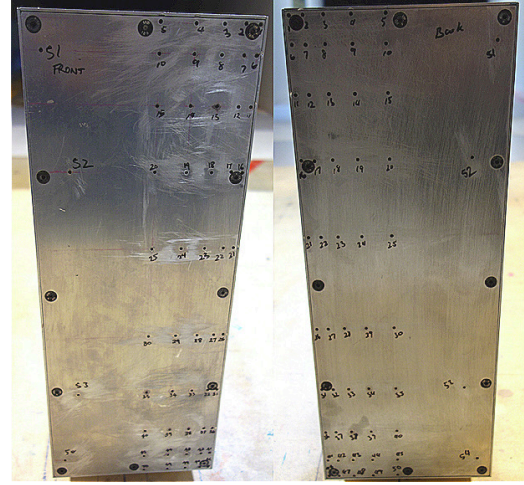


Figure 3: Pressure tap setup on the front (left) and rear (right) surfaces.

sure coefficient is defined in equation 1. (C_p : pressure coefficient, P : pressure, P_{dyn} : dynamic pressure corrected, P_0 : static pressure)

$$C_p = \frac{(P - P_0)}{(P_{dyn})} \quad (1)$$

Results and discussion

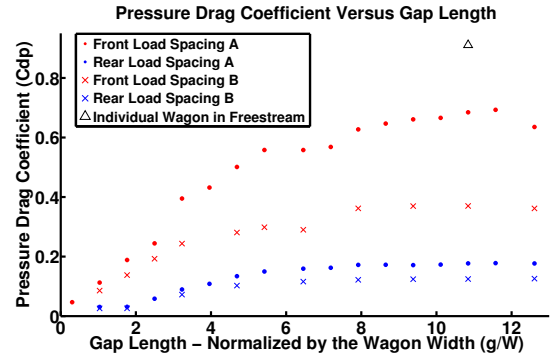


Figure 4: Pressure drag coefficient of the test wagon obtained through surface pressure integration.

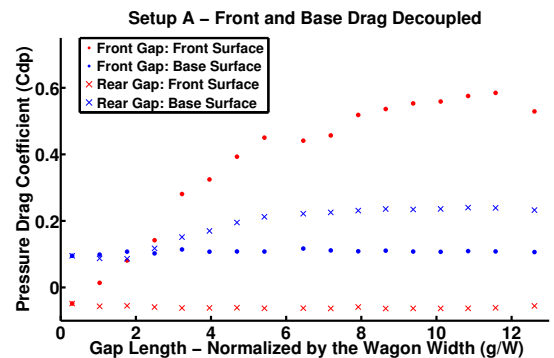


Figure 5: Front and rear pressure drag contributions decoupled.

The obtained pressure coefficient data from the surface pressure tappings is integrated over the surface to obtain the pres-

sure drag coefficient for the test wagon, as shown in figure 4. The individual contribution from the front and rear surfaces to drag is displayed in figure 5. The surface exposed to the gap change will experience an increase in pressure, while the other surface exposed to the constant gap is found to maintain a constant pressure. This suggests that the drag contributions of the front and rear surfaces are effectively decoupled. This is further supported by the drag coefficient produced by the front surface for a constant $12.6W$ front gap and varying rear gap size, see table 1. The front surface in all 3 cases displays similar drag coefficients, although the rear gap sizes are quite different. Given the long length to width of each container, there may be minimal gap flow interaction between the front and rear of the train, causing the pressure on each surface to behave quite independently. In the case of two surface-mounted cubes in tandem with a moderately sized space in between, the oscillating motion in the inter-obstacle gap is coupled with that in the wake of the downstream cube [8]. For larger spacing however, the shear layer from the leading edge of the first cube doesn't reach the second cube, and hence the formation of vortices in the wakes from the two obstacles are then shown to be independent. The wagons in the present study have much larger length to width ratios than a cube, thus any shear layer separating from the wagon should reattach back onto the body before reaching the trailing edge, and is unlikely to interact directly with the downstream wagon.

Pressure Drag Coefficient Comparison	
Load Gap Configuration, Setup A	Front Surface C_{Dp}
Front Gap = $12.6W$, Rear Gap = $0.3W$	0.529
Front Gap = $12.6W$, Rear Gap = $6.46W$	0.525
Front Gap = $12.6W$, Rear Gap = $12.6W$	0.529

Table 1: Front surface pressure drag coefficient for 3 significantly different rear gap sizes.

For load spacing setup A, the contribution to the drag of the wagon caused by the rear gap was approximately 20 - 30% of the drag produced by an equivalent sized front gap. While for load spacing setup B, the drag produced by the rear gap was approximately 30 - 40% of that produced by an equivalent sized front gap. Therefore, from the perspective of the test wagon at least, it would be ideal to avoid having a large front load spacing.

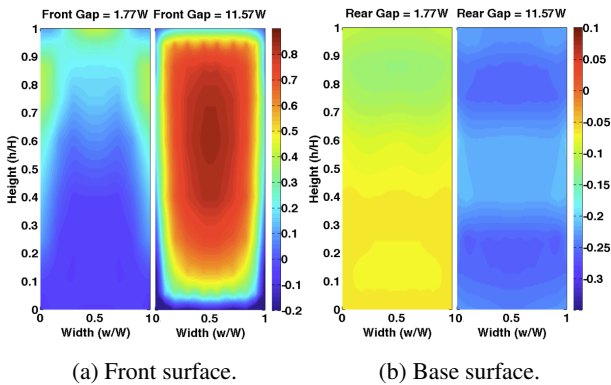


Figure 6: Pressure distribution of setup A. Note: In (a) rear gap = $0.3W$, and for (b) front gap = $0.3W$.

Figure 6(a) illustrates the pressure distribution of the front surface for a front gap size of $1.77W$ and $11.57W$ in setup A. The rear gap size for both cases is $0.3W$. Note that all pressure distributions presented are reflected across the vertical centreline of

the surface. For the baseline configuration, where the gap sizes are $0.3W$, both front and base surfaces display overall negative pressure distributions, indicating suction surfaces. For the front surface, the top and upper section at the sides immediately begins to show transition into positive pressure when the front gap size is increased to $1.04W$. With a progressive increase in the gap size, the region of positive pressure and thus overall drag on the wagon continues to grow. The position of the stagnation point shifts downwards towards the middle of the surface for larger gap spacings. The base pressure distribution remains constant, confirming that only the surface with gap size being varied will contribute to a variation in the overall drag. The rate of increase in the drag tapers off after a front gap size of $7.19W$, with the corresponding pressure distribution displaying only small changes from that point on. Similar growth in pressure on the front surface could be observed for front gap variation in setup B, however the lower half of the surface pressure maintained a negative value due to the shielding from the single stacked container. The drag coefficient is consequently always lower compared to those seen for the front load space variation in setup A. The tapering off of drag growth also occurs earlier at a gap size of $3.23W$, eventually reaching a plateau at a gap size of $7.92W$.

The pressure distribution for a rear gap size of $1.77W$ and $11.57W$ in setup A is shown in figure 6(b), while the front gap size are $0.3W$. For all cases of rear load gaps in setup A, the base maintained a suction surface, and for larger gap spacings of $5.42W$ onwards, three well-defined pressure regions are established, as shown in the righthand plot of figure 6(b). During which these three pressure regions appear, the strength of the suction on the base surface and the drag coefficient of the wagon begins to plateau. It is interesting to note that the drag coefficient displays an initial drop with an increase of rear load spacing; this property can be seen in the pressure profile for the rear gap size of $1.77W$ in figure 6(b), where the yellow region reflects the slight increase in the base pressure.

The drag coefficients obtained in this study for a double-stacked wagon in free-stream is 0.91 , making good agreement with drag coefficients documented in other related studies. Osth and Krajinovic [9] obtained a drag coefficient of 0.904 for a single-stacked wagon. Hammit [4] reports a drag coefficient of approximately 0.8 at a Reynolds number of 10^6 for a single-stacked wagon with a smooth under-carriage. In addition, a drag coefficient of 0.9 has been reported from a wind tunnel measurement of a single 1:3 scaled container wagon with detailed geometry [10].

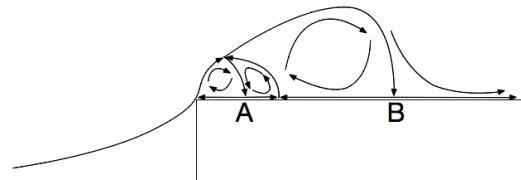
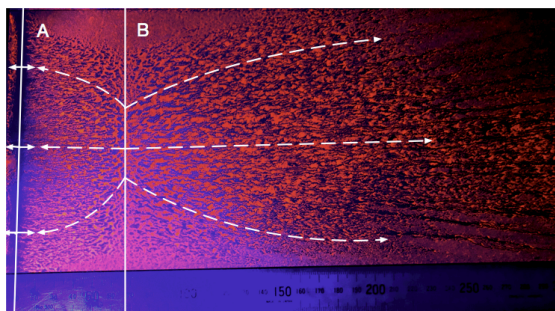


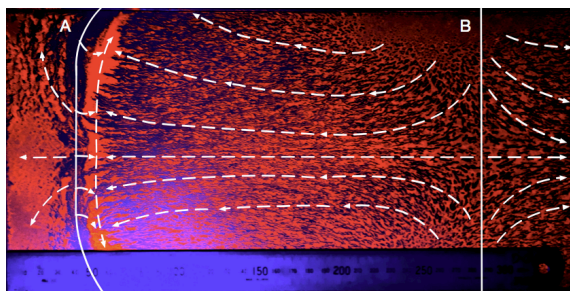
Figure 7: Side-view schematic of the proposed recirculating flow structure at the top of the wagon after [8].

Top-surface flow visualisation suggests a flow structure with 3 recirculation regions, delineated by two reattachment lines A and B and an implied separation line (not captured). This is surmised from the surface visualisation of figure 8. A schematic describing the side view of the proposed flow structure is depicted in figure 7, in line with Martinuzzi and Tropea's [7] depiction of the flow structure at the leading-edge of a surface-mounted cube. For a load spacing of $3.23W$, figure 8(a) shows

that the flow reattaches onto the surface at lines A and B, with the strength of the flow at B notably stronger than A. The fluid travelling from lines A and B towards each other is conjectured to meet just slightly downstream of line A. Increasing of front gap spacing results in lines A and B shifting downstream, and at the same time moving further apart. This is seen in figure 8(b), where the recirculation region becomes larger and increases in strength. For the flow structure corresponding to a gap size of $9.38 W$, surface fluid travelling away from line B displays a converging and then diverging pattern from the centreline, in contrast to the previous case where the flow diverges immediately towards the sides when travelling away from B. Reattachment line A shows signs of curvature towards the sides of the wagon. This feature was present for gap length of $6.46 W$ and greater. The meeting of surface flows from lines A and B were clearly defined by lines of deposited clay, in addition, it appears that upon meeting, those clay particles are siphoned away from the centreline towards the sides of the wagon. The above-mentioned properties are difficult to observe for gap sizes less than $3.23 W$, as the physical flow features are too close to be distinguishable, although further experiments may resolve this issue.



(a) Front gap = $3.23 W$.



(b) Front gap = $9.38 W$.

Figure 8: Clay skin friction visualisations for the top surface of the test wagon.

Conclusion

A key conclusion is that for equivalent front and rear load gap sizings, the front gap induces a much larger drag on the test wagon than the rear gap. For the particular sized wagon investigated—a $1/14.6$ th-scale model of a 48ft long wagon—the cavity flow in the front and rear gaps appear to behave independently. Therefore, the pressure exerted on each surface is a function of its own corresponding gap size. While at smaller gap sizes, the drag produced by setup A was only slightly bigger than setup B, the drag penalty for setup A was significantly greater for larger load spacing, especially for front gap variation. For large gaps, the pressure profiles of the front and rear surface resembled those of a surface mounted-cube quite closely. The recirculation region at the leading edge of the top

surface consists of three main recirculation regions, similar to those observed on surface mounted cubes. The size of the recirculation region was a function of the front gap size. Due to the length of the wagon, reattachment of the flow back onto the surface always occurs well before the trailing edge.

Acknowledgement

This research was supported by Pacific National and Australian Research Council's Linkage Projects funding scheme, project number LP13100953.

References

- [1] Engdahl, R., Gielow, R. and Paul, J., Train resistance-aerodynamics.: Volume i of ii. intermodal car application, in *RAILROAD ENERGY TECHNOLOGY CONFERENCE II (1986:)*, 1987.
- [2] Gielow, M. and Furlong, C., Results of wind tunnel and full-scale tests conducted from 1983 to 1987 in support of the association of american railroads' train energy program, Technical report, 1988.
- [3] Golovanevskiy, V. A., Chmovzh, V. V. and Girka, Y. V., On the optimal model configuration for aerodynamic modeling of open cargo railway train, *Journal of Wind Engineering and Industrial Aerodynamics*, **107**, 2012, 131–139.
- [4] Hammitt, A., Aerodynamic forces on freight trains. volume 1: Wind tunnel tests of containers and trailers on flatcars, Technical report, 1976.
- [5] Lai, Y.-C. and Barkan, C. P., Options for improving the energy efficiency of intermodal freight trains, *Transportation Research Record: Journal of the Transportation Research Board*, **1916**, 2005, 47–55.
- [6] Lai, Y.-C., Barkan, C. P. and Önal, H., Optimizing the aerodynamic efficiency of intermodal freight trains, *Transportation Research Part E: Logistics and Transportation Review*, **44**, 2008, 820–834.
- [7] Martinuzzi, R. and Tropea, C., The flow around surface-mounted, prismatic obstacles placed in a fully developed channel flow (data bank contribution), *Journal of Fluids Engineering*, **115**, 1993, 85–92.
- [8] Martinuzzi, R. J. and Havel, B., Turbulent flow around two interfering surface-mounted cubic obstacles in tandem arrangement, *Journal of fluids engineering*, **122**, 2000, 24–31.
- [9] Östth, J. and Krajnović, S., A study of the aerodynamics of a generic container freight wagon using large-eddy simulation, *Journal of Fluids and Structures*, **44**, 2014, 31–51.
- [10] Peters, J.-L., Effect of reynolds number on the aerodynamic forces on a container model, *Journal of Wind Engineering and Industrial Aerodynamics*, **49**, 1993, 431–438.
- [11] Watkins, S., Saunders, J. and Kumar, H., Aerodynamic drag reduction of goods trains, *Journal of Wind Engineering and Industrial Aerodynamics*, **40**, 1992, 147–178.